A STUDY ON THE EFFECT OF THE DIE TRANSVERSE ANGLE AND THE PART ROTATIONAL FEED ANGLE IN THE COLD RADIAL FORGING PROCESS OF RODS

Mozhdeh Fattahpoor Roushan, Hamed Afrasiab[*], Ramazan Ali Jafari Talookolaei

[*] Corresponding author (afrasiab@nit.ac.ir)

Mechanical Engineering Department, Babol Noshirvani University of Technology
Babol, Iran
Email: afrasiab@nit.ac.ir

Tel.: +98-11-35501321

Fax: +98-11-32334201

ABSTRACT

Radial forging is an efficient and high-precision process for manufacturing rotary parts such as shafts, axles, and gun barrels. While this process has been extensively investigated in the literature, effect of some parameters like the die transverse angle and the part rotational feed angle has not been adequately studied since simulating several steps of this process with a full three-dimensional model is required for this purpose which is labor-intensive and time-consuming. To bridge this gap, in this paper a three-dimensional nonlinear finite element model has been developed to analyze effects of the die transverse angle and part rotational feed angle in this process. To address the lack of reliable experimental data in the literature, an innovative approach has been proposed and used for validation of the developed finite element model. It has been observed that dies with transverse angle of 155° and 165° provide the best performance in producing a part geometry close to the desired shape. However, the most uniform residual stress distribution is obtained in forging by a die with a smaller transverse angle. Furthermore, for improving the shape and quality of the final product, the part rotational feed angle should be reduced as much as possible.

Keywords: Radial forging process; Die transverse angle; Part rotational feed angle; Residual Stress; Product quality.

1. INTRODUCTION

Radial forging is an open-die forging process used for reducing the diameter of shafts, tubes and axles and for creating internal profiles for tubes such as rifling the gun barrels [1]. The advantages of the radial forging process lie in its capability to produce superior mechanical properties in the product, tight dimensional and geometrical tolerances, good surface finish, high production rate and material saving [2].

Normally, in radial forging four hammer dies are radially arranged around the part. The part is shaped by impact of dies moving reciprocally with short course and high frequency.
The part displacement in the radial forging process consists of both translational and rotational motions [3]. The translational component is performed to feed the part through the dies and the rotational motion is to achieve a round circular shape. Both of these motions are stopped during die-part contact to avoid part from twisting. Three principal movements of the part and dies are depicted in Figure (1).
A longitudinal cut of the radial forging die is shown in Figure (2-a). Angle α in this figure is the die inlet angle. The front view of the die is presented in Figure (2-b). The die may have a curved or a bilinear lateral profile as can be seen in this figure. In a die with bilinear profile, the angle β between the lines is called the transverse angle.
Different parameters affect the outcome of the radial forging process. The radius reduction ratio, the die geometry, and the part rotational and axial feeds are among these parameters. On the other hand, different operational characteristics such as the forming force [4], uniformity of the strain distribution [5], residual stresses [6] and tool life [1] are usually investigated in the literature to evaluate the performance of this process. Among these operational characteristics, the strain and residual stress distributions are of particular importance due to their effect on the dimensional stability, mechanical properties and operational life of the process product [7].
The radial forging process has been generally studied by one of the analytical or finite element method (FEM) approaches in the literature. Among the most popular analytical approaches, the slab method [2,7], the upper-bound method [8], and most recently the asymptotic analysis can be mentioned. For instance, Afrasiab [9] conducted an improved upper bound analysis to predict the void closure behavior in the metal billets. In another study, Afrasiab et al. [10] proposed an analytical approach based on the asymptotic analysis to develop an axisymmetric model for the radial forging process of rods. While analytical approaches can provide a fast means to obtain the solution, none of them are as accurate and powerful as the finite element method. Subsequently, many articles have employed this method for studying different aspects of the radial forging process. For instance, Afrasiab and Movahhedy [1] studied the effect of different parameters on the tooling life by a 3D FEM model. In another study [7], Afrasiab used 3D finite element method for improving the die design in radial forging of tubes without a mandrel. Darki and Raskatov [11] conducted a symmetric 3D finite element simulation to

obtain the cantors of residual stress (RS), strain velocity, and temperature; and to explore the influence of friction parameters on the contact force, stresses, and equivalent strains. Wang and Dong [12] developed a FEM model to study the influence of Lode parameter on the void evolution behavior of the power-low viscous solids in the radial forging process. Yang et al. [13] focused on the effect of the cold radial forging on the forged steel tube under different forging reductions. Xu et al. [14] investigated the evolution of the residual stress during annealing of steel tube processed by cold radial forging. Zuev et al. [15] examined the effect of radial forging on the mechanical properties of Ti-based alloys. Zou et al. [16] studied the deformation mechanism of ZK60 magnesium bars during the radial forging. Microstructural and mechanical response of ZK60 magnesium alloy subjected to radial forging was considered by Zou et al. [17] in another study. Yang et al. [18] employed a two-dimensional polycrystalline finite element model to simulate the microstructure and the texture of the 30SiMn2MoVA steel gun barrel processed by radial forging. Makiyama [19] conducted a finite element simulation using commercial software FORGE to study the effect of rotational feed emulating four-die radial forging on the forged shape in mandrel-less incremental forging of thick circular tube. Darki and Raskatov [20] developed a 3D visco-elastoplastic finite element model to predict the effect of the die angle on the forging load and the residual stresses in the workpiece. Mackey et al. [21] used a finite element model of the radial forging process with cohesive zones to simulate the evolution of non-metallic inclusions during the forging process. Despite many studies performed previously on the radial forging process, some aspects of the process still need further attention. For example, an overview on the related literature shows that while the effect of parameters such as the die inlet angle, its land length, the axial feed, and the friction conditions have been extensively investigated in the literature, a comprehensive study on the effect of important parameters such as the die transverse angle or the part rotational feed has been never performed. Furthermore, in most previous studies even the most recent ones the effect of the rotational feed is neglected and the variation of the die shape in the cross-section is ignored [10,13]. This is due the fact that a full 3D model of the process is required for including these parameters in the analysis. Such a model is more complex to develop and consumes more computational time and resources. Considering this fact, a nonlinear 3D finite element model of the radial forging process developed and used in this paper to study the effect of the die transverse angle and part rotational feed on the plastic

equivalent strain and residual stress distribution in the part. These parameters are among the most important factors affecting the final product quality. Since reliable and accurate experimental data for the radial forging process are not presented in the existing literature, an innovative experimental procedure based on two simple compression tests has been designed and implemented for verification of the developed finite element model.

Based on the above discussion, the main novelties of the current study are:

1- development of a nonlinear 3D finite element model for study of the effect of the die transverse angle and part rotational feed in the radial forging process for the first time,
2- introducing a new simple and innovative experimental method for verifying the theoretical models of the radial forging process.

Detailed description of the procedures is given in the following sections.

2. METHODS

2.1 Finite element model

In order to study the radial forging process, a nonlinear 3D finite element model is developed in the framework of ABAQUS/Explicit commercial software. The formulation governing this model, after linearization, can be written as:

$$\left[M^e\right]\left\{\ddot{U}^e\right\}+\left[K^e\right]\left\{U^e\right\}=\left\{F^e\right\} \quad (1)$$

In these equations, $\left[M^e\right]$ and $\left[K^e\right]$ are the mass and stiffness matrices, respectively, $\left\{F^e\right\}$ denotes the mechanical force vector, $\left\{U^e\right\}$ and $\left\{\ddot{U}^e\right\}$ are the displacement and acceleration vectors, respectively.

It is known that any element that locks volumetrically, like first order brick elements (C3D8), will not perform well for von Mises plastic materials which are nearly incompressible. Reduced integration is generally used to eliminate volumetric locking common in modeling incompressible or nearly incompressible materials. Consequently, in this paper, first order brick elements with reduced integration (C3D8R) are used to mesh the part (modeled as von Mises elastic-plastic material) to avoid numerical problems associated with volumetric locking such as divergent or less accurate solutions. Since dies deformation is negligible, they are assumed to be rigid bodies in the FEM model and are meshed by rigid 1st order brick elements. The meshed assembly of the part and dies is shown in Figure (3).

The process can be assumed as isothermal since the process is performed at room temperature

and the heat generated during the plastic forming of the part dissipates due to heat exchange with surroundings and dies. A compression test was conducted on a sample made from the part material which is ST37 steel. The stress-strain curve shown in Figure (4-a) was obtained in this test. The raw data related to this compression test is included in the supplementary material. The axial and rotational feeds were applied to each die reference point as boundary conditions. The axial feed and forging frequency were set equal to 1 mm per stroke [22] and 680 hits per minute [23], respectively. The initial and final diameters of the workpiece were assumed to be 15.5 mm and 11.1 mm. Each die moved a distance of 2.2 mm in each stroke, however, since the dies were steep the amount of diameter reduction in each stroke was dependent on the workpiece axial location under the dies. It was also assumed that supports apply no front-pull and back-push forces at workpiece ends [22].

A constant pressure of $30\,\mathrm{MPa}$ was imposed at tube ends to account for back pressure applied by the chuck heads on the tube. This boundary condition was previously proposed in [24].

The Coulomb friction law, expressed as $\tau = \mu p$ where τ is the frictional shear stress and p is the normal stress [1], was used to define the friction at the part-dies interface. The ring compression test was used to measure the coefficient of friction, μ. The ring compression test is a standard procedure for determining the friction coefficient in metal forming processes. In this test, a circular ring is axially compressed between two flat dies, which in this paper are the pressure pads of the universal test machine used for performing experimental tests. For a given height reduction, the deformation behavior of the internal diameter of the test specimen can be used to determine the magnitude of the friction coefficient at the die/workpiece interface. Specific calibrated curves can be used to determine the friction coefficient for different values of the inner diameter change and the ratio of compression [25]. The value of $\mu = 0.2$ was obtained by the ring compression test in this paper.

2.2 Mesh independence test

A mesh independence test has been implemented to ensure an optimum mesh in the in the finite element model. The maximum value of the von Mises stress in the part was compared in meshes with different element density. The obtained results presented in Figure (4-b) indicate that a mesh of 58320 elements is a suitable choice. The maximum von Mises stress was observed on the workpiece surface which has the maximum deformation in contact with dies.

2.3 Verification of the finite element model

Normally, numerical models are verified by comparing simulation results with experimental data. Regarding the radial forging process, while numerical and analytical approaches has been widely used to study this process, reliable experimental data are very scarce in the literature. In view of this shortcoming, some authors, e.g. in [26,27], opted to use experimental data reported in a PhD dissertation [28] for verification of numerical and analytical models of the radial forging process. But these experimental data are very old and above all are not reported for the radial forging itself, but for the radial swaging which bears some similarity to the radial forging process. Consequently, the accuracy of such verifications is disputed.

In order to address this shortcoming, here an innovative approach is presented. To this end, Figure (5-a) illustrates the first forming step in the four-die radial forging process. In this step, two opposite dies hit the lateral surface of the part and then return to their starting position. In the next step according to Figure (5-b), two other dies lying perpendicular to the path of the first dies hit the part and move back to their initial position.

The final product is shaped by multiple hits of dies in combination with part axial and rotational feeds. Therefore, if one only considers the first two hits of dies, the radial forging process is equivalent to a set of two simple compression tests. In the first test shown in Figure (6-a), the lateral surface of a cylindrical sample is flattened by pressure pads of a universal test machine.

In the second step, the sample is rotated by an angle of 90^{o} and the first step is repeated as shown in Figure (6-b).

Since the strain rate effect is negligible at room temperature, the above-described radial forging steps and compression tests are equivalent regardless of the part forming speed. Considering this equivalence, the finite element model of the radial forging process can be verified against experimental data taken from the equivalent compression tests.

Figure (7-a) shows, from left to right, the original sample, the sample after performing the first compression test, and the sample after the second compression test. The finite element model of the part in the equivalent radial forging process is also shown in Figure (7-b) before and after first two hits of dies. The sample was made of st37 steel with diameter of 15.5 mm and length of 35 mm. Dies had inlet angle of 0^{o} and transverse angle of 180^{o} in the FEM simulation.

Figures (8-a) and (8-b) compare the forming force obtained in the finite element simulation

with corresponding experimental data. The finite element and experimental results are in good agreement as shown in these figures.

3. Results and discussion

In this section, the effect of the die transverse angle, β, and the part rotational feed angle, ϕ, is investigated on the final shape and some quality attributes of the radial forging product. The values considered for these parameters are listed in table 1. A 3D plot of the path on which results are presented is also given figure (9-a). The hoop and axial stresses (σ_θ and σ_r) are defined according to Figure (9-b).

One of the most important characteristics of all metal forming processes is their capability to form parts as close as possible to the final desired shape. In order to measure this characteristic, a new parameter called the percentage of normalized area difference is defined as:

$$A_n = \frac{A_{\text{forged part}} - A_{\text{desired product}}}{A_{\text{desired product}}} \times 100 \qquad (2)$$

where $A_{\text{forged part}}$ and $A_{\text{desired product}}$ are the cross-sectional area of the forged part and desired product, respectively. The hypothetical cross sections of the desired product and the forged part are presented in Figures (10-a) and (10-b). If these two cross sections are overprinted as shown in Figure (10-c), A_n is equal to the area of the hatched surface divided by the area shown in Figure (10-a) multiplied by 100.

Regarding this definition, a lower value for A_n means that the part formed closer to its desired shape.

3.1 Effect of the die transverse angle on A_n

Figure (11-a) shows variation of A_n versus die transverse angle, β, after two hits of dies. According to this figure, in smaller values of β a lower A_n is obtained and the part gets closer to its desired shape. This result seems logical since by reduction of β, die better encircles the part and creates greater plastic deformation inside it. A view of the deformed part after two hits of dies is shown in Figure (12-a) for $\beta = 135^o$ and $\beta = 180^o$.

Variation of A_n with β after a complete circle rotation of the part is shown in Figure (11-b) for rotational feed angle of $\phi = 11.25^o$. According to this figure, dies with $\beta = 155^o$ and $\beta = 165^o$ form part closer to its desired shape. The normalized area difference between the forged part and

the desired product is about 0.3% or 0.003 in forging with these dies. The die with $\beta = 180^o$ has the worst performance in this respect. A negative value for A_n in forging by a die with $\beta = 180^o$ may not be expected. This result likely stemmed from the coupled effect of the die transverse angle and rotational feed and authors found it very difficult to explain.

A_n is negative for dies with $\beta = 135^o$ and $\beta = 180^o$. This means that the product cross section becomes smaller than its desired value in forging with these dies. Positive value of A_n for other transverse angles means that the product cross section is larger than the desired one for these dies. The deformed cross section of parts forged by dies with $\beta = 135^o$ and $\beta = 180^o$ is shown in Figure (12-b) for $\phi = 11.25^o$.

It is worth mentioning that as reported in [29] for rotary feeds of 45°, 22.5° and 11.25°, a total rotation angle of 360° (a complete circle rotation) seems to be sufficient for finalizing the strain and residual stress distribution in the workpiece and obtaining the product desired shape. More discussion about this subject is also present in [29].

3.2 Effect of the part rotational feed angle on A_n

Variation of the normalized area difference with rotational feed angle is shown in Figure 13. Three rotational feed angles of $\phi = 11.25^o, 22.5^o, 45^o$ are considered for this purpose. According to this figure, A_n is smaller for smaller values of ϕ which means that the part get closer to its desired shape. It can also be seen in Figure 14 that the cross section of the part forged with $\phi = 45^o$ is not a true circle but a polygon.

3.3 Effect of the die transverse angle on the equivalent plastic distribution

The equivalent plastic strain distribution in the part has a profound impact on its mechanical properties. Owing to the strain-hardening effect, the part mechanical strength increases with increasing the equivalent plastic strain. Moreover, a more uniform distribution of plastic strain leads to uniformity of mechanical properties, improved residual stress distribution and dimensional stability of the process product.

Figure (15-a) shows distribution of the equivalent plastic strain in the hoop direction of the part surface for dies with different transverse angles. According this figure, the equivalent plastic strain in the hoop direction is not meaningfully affected by the die transverse angle. Only the transverse angle of $\beta = 180^o$ may be preferred since it makes a larger plastic strain in the part.

Distribution of the equivalent plastic strain in the radial direction of the part is presented in Figure (15-b). As this figure shows, the maximum mean value of the plastic strain distribution occurs in the die with $\beta = 180^{o}$, while the maximum uniformity is obtained in forging by a die with $\beta = 165^{o}$. It should be noted that the mean value of the plastic strain distribution is 0.34 for $\beta = 135^{o}$ and 0.38 for $\beta = 180^{o}$.

Data of Figure (16-a) are for a radial direction that lies at $\theta = 180^{o}$. It should be indicated that while variation of the equivalent plastic strain in other radial directions is different quantitatively, it shows almost similar qualitative trend (higher strain values in the path start and end points and lower values in the path midpoints) in all radial directions.

The contour of the equivalent plastic strain in parts forged by dies with $\beta = 135^{o}$ and $\beta = 180^{o}$ is shown in Figure (16-a) and (16-b), respectively.

3.4 Effect of the part rotational feed angle on the equivalent plastic strain

Figure (17-a) shows the equivalent plastic strain distribution in the hoop direction of the part surface for different values of the rotational feed angle. According to this figure, a larger plastic strain is made in smaller rotation angles. This may be the consequence of the fact that in smaller rotational feeds, the part withstands more die hits and therefore plastic strain before completing full circle rotation.

3.5 Effect of the die transverse angle on the residual stress distribution

Residual stresses directly affect the part life and performance depending on their sign and magnitude. For example, tensile residual stresses cause fatigue cracks to start and grow and consequently shorten the working life of the part under dynamic loading. Compressive stresses, on the other hand, prevent fatigue cracks to initiate and develop. Furthermore, residual stresses affect the dimensional stability of the part and may cause undesired deformation.

Fatigue cracks usually nucleate at the part surface where stresses are highest and where a corrosive environment and geometry changes exist. As a result, stress distribution on the part surface is of prime importance. The die transverse angle effect on the residual von Mises distribution in the hoop direction of the part surface is presented in Figure (17-b). It can be seen in this figure that residual stresses are more uniform in parts forged by dies with smaller transverse angle. Consequently, higher dimensional stability is expected in these parts.

Figures (18-a) and (18-b) represent the effect of the die transverse angle on the residual hoop and axial stresses on the part surface for inlet angle of $\alpha = 10^{o}$ and feed angle of $\phi = 11.25^{o}$. According to these figures, the hoop stress distribution is compressive and very similar for all values of the transverse angle. The axial stress is also compressive in most points of the part surface and the best distribution is obtained in forging by a die with $\beta = 165^{o}$ where compressive stresses are created everywhere in the part surface. Compressive hoop and axial stresses developed in most surface points of parts forged by radial forging process are evidences for superiority of this process for reducing the part diameter compared with processes such as turning. It can also be seen in figure (18) that the maximum residual hoop stress occurs at a point with $\theta = 90^{o}$. This point lies in the middle of two dies applying the first hits on the part and consequently experiences the maximum deformation in the hoop and radial directions in the first hit. The first hit of dies is important since the maximum deformation of part occurs in this hit.

3.6 Effect of the part rotational feed angle on the residual stress distribution

Diagrams of von Mises, hoop and axial residual stress distribution in the part surface are shown in Figures (19) and (20), respectively, for different values of rotational feed angle. According to these figures, the most uniform and the most compressive stress distributions are obtained in $\phi = 45^{o}$ and $\phi = 11.25^{o}$, respectively.

4 CONCLUSION

In this paper, the finite element method was employed to comprehensively study the effect of the die transverse angle and the part rotational feed angle in the radial forging process for the first time. For this purpose, several steps of the process were simulated by developing a full 3D nonlinear FEM model of this process in the Abaqus software. An innovative experimental approach was also introduced to verify the FEM model of the process. The results of this study demonstrated that the dies with transverse angle of 155° and 165° form the part closest to its final shape. Furthermore, the cross-sectional area of the product forged by dies with transverse angle of 145°, 155° and 165° are slightly bigger than desired value, while this area is smaller than desired value in forging by dies with transverse angle of 135° and 180°. The die transverse angle has a minor effect on the equivalent plastic strain distribution in the hoop direction. But in the radial direction, the largest plastic strain is created by transverse angle of 180° and the most uniform plastic strain by transverse angle of 135°. The von Mises stress is more uniform in parts

forged by dies with smaller transverse angle and increasing the die transverse angle reduces the residual stress uniformity. Reducing the part rotational feed angle leads to development of higher plastic strain and residual stress in the part surface. Furthermore, it makes residual hoop and axial stresses more compressive.

Nomenclature

$A_{\text{desired product}}$	Cross-sectional area of the desired product
$A_{\text{forged part}}$	Cross-sectional area of the forged part
A_n	Percentage of normalized area difference
$\{U^e\}$	Displacement vector
$\{\ddot{U}^e\}$	Acceleration vector
F^e	Mechanical force vector
K^e	Finite element stiffness matrix
M^e	Finite element mass matrix
p	Normal stress
β	Die transverse angle
μ	Coefficient of friction
τ	Frictional shear stress
ϕ	Part rotational feed angle

References

1. Afrasiab, H. and Movahhedy, M. R., "9-Numerical study of the effects of process parameters on tool life in a cold radial forging process - ProQuest", *Scientia Iranica. Transaction B, Mechanical Engineering*, **21**(2), pp. 339–346 (2014).
2. Afrasiab, M., Afrasiab, H., Movahhedy, M. R., and et al., "Design of the die profile for the incremental radial forging process", *Iranian Journal of Science and Technology Transactions of Mechanical Engineering*, **39**(0), pp. 89–100 (2015).
3. Li, Y., He, T., and Zeng, Z., "Numerical simulation and experimental study on the tube sinking of a thin-walled copper tube with axially inner micro grooves by radial forging", *Journal of Materials Processing Technology*, **213**(6), pp. 987–996 (2013).
4. Azari, A., Poursina, M., and Poursina, D., "4-Radial forging force prediction through MR, ANN, and ANFIS models", *Neural Comput & Applic*, **25**(3–4), pp. 849–858 (2014).
5. Sanjari, M., Saidi, P., Karimi Taheri, A., and et al., M., "7-Determination of strain field and heterogeneity in radial forging of tube using finite element method and microhardness test", *Materials & Design*, **38**, pp. 147–153 (2012).

6. Sahoo, A. K., Tiwari, M. K., and Mileham, A. R., "8-Six Sigma based approach to optimize radial forging operation variables", *Journal of Materials Processing Technology*, **202**(1), pp. 125–136 (2008).
7. Afrasiab, H., "10-Numerical and analytical approaches for improving die design in the radial forging process of tubes without a mandrel", *Scientia Iranica Transactions B: Mechanical Engineering*, **23**(1) (2016).
8. Yang, X., Dong, X., and Wu, Y., "1-An upper bound solution of forging load in cold radial forging process of rectangular cross-section billet", *Int J Adv Manuf Technol*, pp. 1–12 (2017).
9. Afrasiab, H., "An improved upper bound analysis for study of the void closure behavior in the plane strain extrusion", *Mechanics Research Communications*, **124**, p. 103971 (2022).
10. Afrasiab, H., Hamzekolaei, M. G., and Hassani, A., "New insight into the radial forging process by an asymptotic-based axisymmetric analysis", *Applied Mathematical Modelling*, **102**, pp. 811–827 (2022).
11. Darki, S. and Raskatov, E. Y., "Analysis of the hot radial forging process according to the finite element method", *Int J Adv Manuf Technol*, **110**(3–4), pp. 1061–1070 (2020).
12. Wang, X. and Dong, X., "A void evolution model accounting for stress triaxiality, Lode parameter and effective strain for hot metal forming", *International Journal of Mechanical Sciences*, **168**, p. 105309 (2020).
13. Yang, Y., Fan, L., and Xu, C., "The microstructure, texture evolution and plasticity anisotropy of 30SiMn2MoVA high strength alloy steel tube processed by cold radial forging", *Materials Characterization*, **169**, p. 110641 (2020).
14. Xu, W., Mo, J., Zhang, J., and et al., "Evolution of Residual Stress and Microstructure during Annealing of 30SiMn2MoVA High-Strength Alloy Steel Tube Processed by Cold Radial Forging", *J. of Materi Eng and Perform*, **30**(8), pp. 5889–5897 (2021).
15. Zuev, L. B., Shlyakhova, G. V., and Barannikova, S. A., "Effect of Radial Forging on the Microstructure and Mechanical Properties of Ti-Based Alloys", *Metals*, **10**(11), p. 1488 (2020).
16. Zou, J., Ma, L., Zhu, Y., and et al., "Deformation mechanism of ZK60 magnesium bars during radial forging: Mathematical modeling and experimental investigation", *Materials Characterization*, **179**, p. 111321 (2021).
17. Zou, J., Ma, L., Jia, W., and et al., "Microstructural and mechanical response of ZK60 magnesium alloy subjected to radial forging", *Journal of Materials Science & Technology*, **83**, pp. 228–238 (2021).
18. Yang, Y., Xu, C., and Fan, L., "Inhomogeneous Deformation and Texture Evolution of 30SiMn2MoVA Steel Gun Barrel Processed by Radial Forging Based on Cross-scale Crystal Plasticity Finite Element Method", *Mat. Res.*, **25** (2022).
19. Makiyama, T., "Effects of Rotational Feed Emulating Four-Die Radial Forging on Forged Shape in Mandrel-Less Incremental Forging of Thick Circular Tube", *Presentations and videos to 16th International Conference on Computational Plasticity (COMPLAS 2021).*, IS02-Applications of Computational Methods to Product and Process Design for Industry (2022).
20. Darki, S., Raskatov, E. Y., and New Material and Technology Institute Ural Federal University, "Development of an Analysis Method for Radial Forging Parameters Based on Hardness Criterion", *JMechE*, **20**(1), pp. 149–167 (2023).

21. Mackey, B. T., Siegmund, T., and Sangid, M., "Simulating the evolution of non-metallic inclusions during the forging process", *Journal of Manufacturing Science and Engineering*, pp. 1–48 (2023).
22. Ghaei, A., Karimi Taheri, A., and Movahhedy, M. R., "25-A new upper bound solution for analysis of the radial forging process", *International Journal of Mechanical Sciences*, **48**(11), pp. 1264–1272 (2006).
23. Fan, L., Wang, Z., and Wang, H., "2-3D finite element modeling and analysis of radial forging processes", *Journal of Manufacturing Processes*, **16**(2), pp. 329–334 (2014).
24. Ghaei, A. and Movahhedy, M. R., "20-Die design for the radial forging process using 3D FEM", *Journal of Materials Processing Technology*, **182**(1), pp. 534–539 (2007).
25. Sofuoglu, H., Gedikli, H., and Rasty, J., "23-Determination of Friction Coefficient by Employing the Ring Compression Test", *J. Eng. Mater. Technol*, **123**(3), pp. 338–348 (2000).
26. Ghaei, A., Movahhedy, M. R., and Karimi Taheri, A., "26-Finite element modelling simulation of radial forging of tubes without mandrel", *Materials & Design*, **29**(4), pp. 867–872 (2008).
27. Alaei, E., Afrasiab, H., and Dardel, M., "Analytical and numerical fluid–structure interaction study of a microscale piezoelectric wind energy harvester", *Wind Energy*, **23**(6), pp. 1444–1460 (2020).
28. Uhlig, A., "28-Investigation of the motions and the forces in radial swaging", Technical University Hannover (1964).
29. Afrasiab, H. and Movahhedy, M. R., "31-Numerical Study of the Workpiece Rotation Effect on the Strain and Residual Stress Distribution in the Cold Radial Forging Process", pp. 785–792 (2010).
30. Hosford, W. F. and Caddell, R. M., *Metal Forming: Mechanics and Metallurgy*, Cambridge University Press (2011).

Fig. 1 Motions in radial forging: (a) dies reciprocal movement, (b) part translation, (c) part rotation (rotational feed)

Fig. 2 a) Longitudinal cut of the die with the inlet angle definition, b) front view of the die with the transverse angle definition

Fig. 3 The meshed assembly of the part and dies

Fig. 4 a) the stress-strain curve obtained for the part material, b) results of the mesh

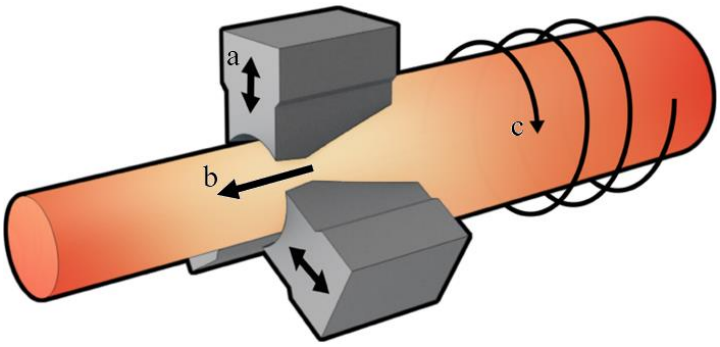

Fig. 1 Motions in radial forging: (a) dies reciprocal movement, (b) part translation, (c) part rotation (rotational feed)

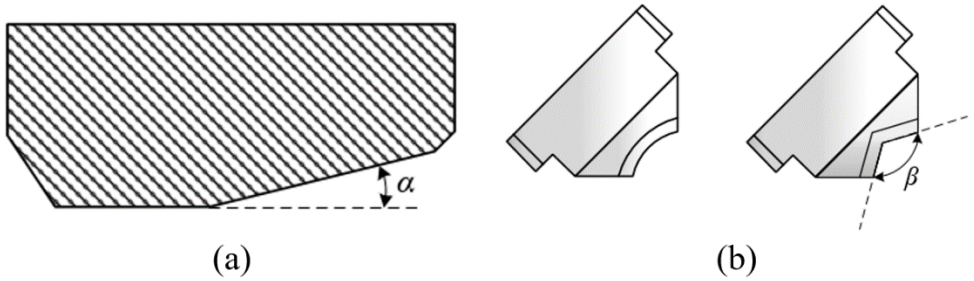

Fig. 2 a) Longitudinal cut of the die with the inlet angle definition, b) front view of the die with the transverse angle definition

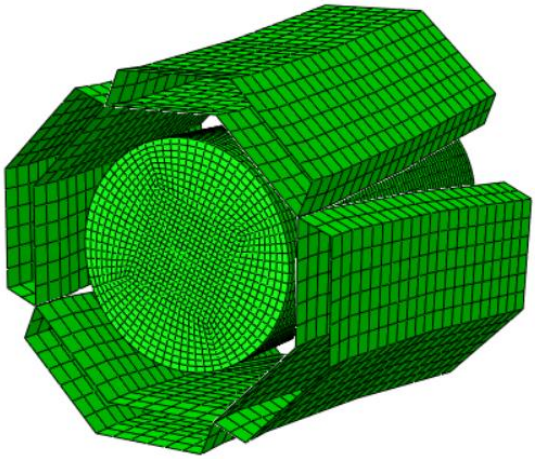

Fig. 3 The meshed assembly of the part and dies

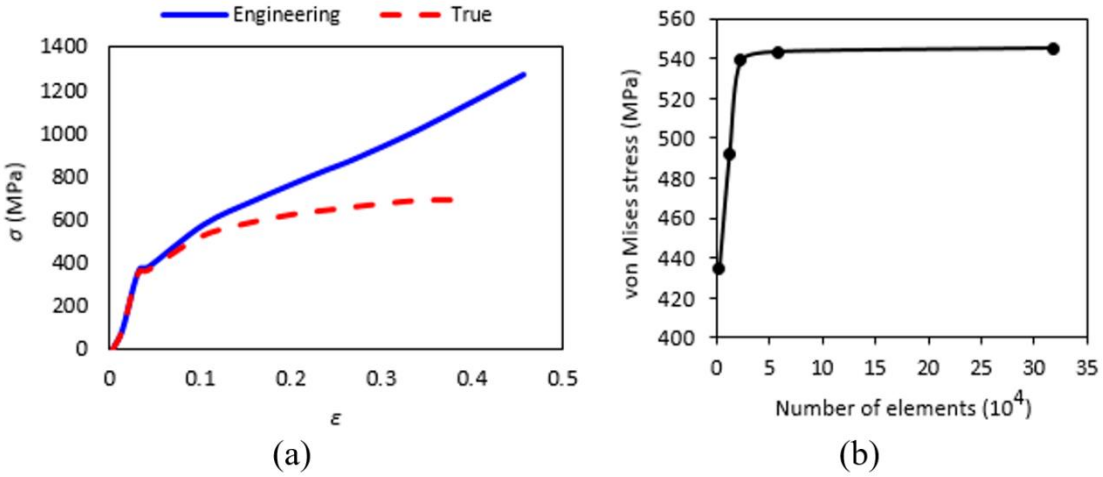

Fig. 4 a) the stress-strain curve obtained for the part material, b) results of the mesh independence test

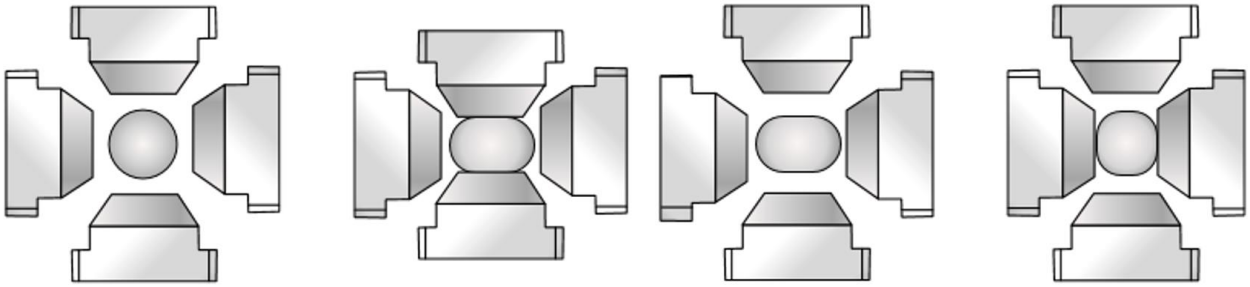

(a) (b)

Fig. 5 a) The first and b) the second hit of dies in the radial forging process

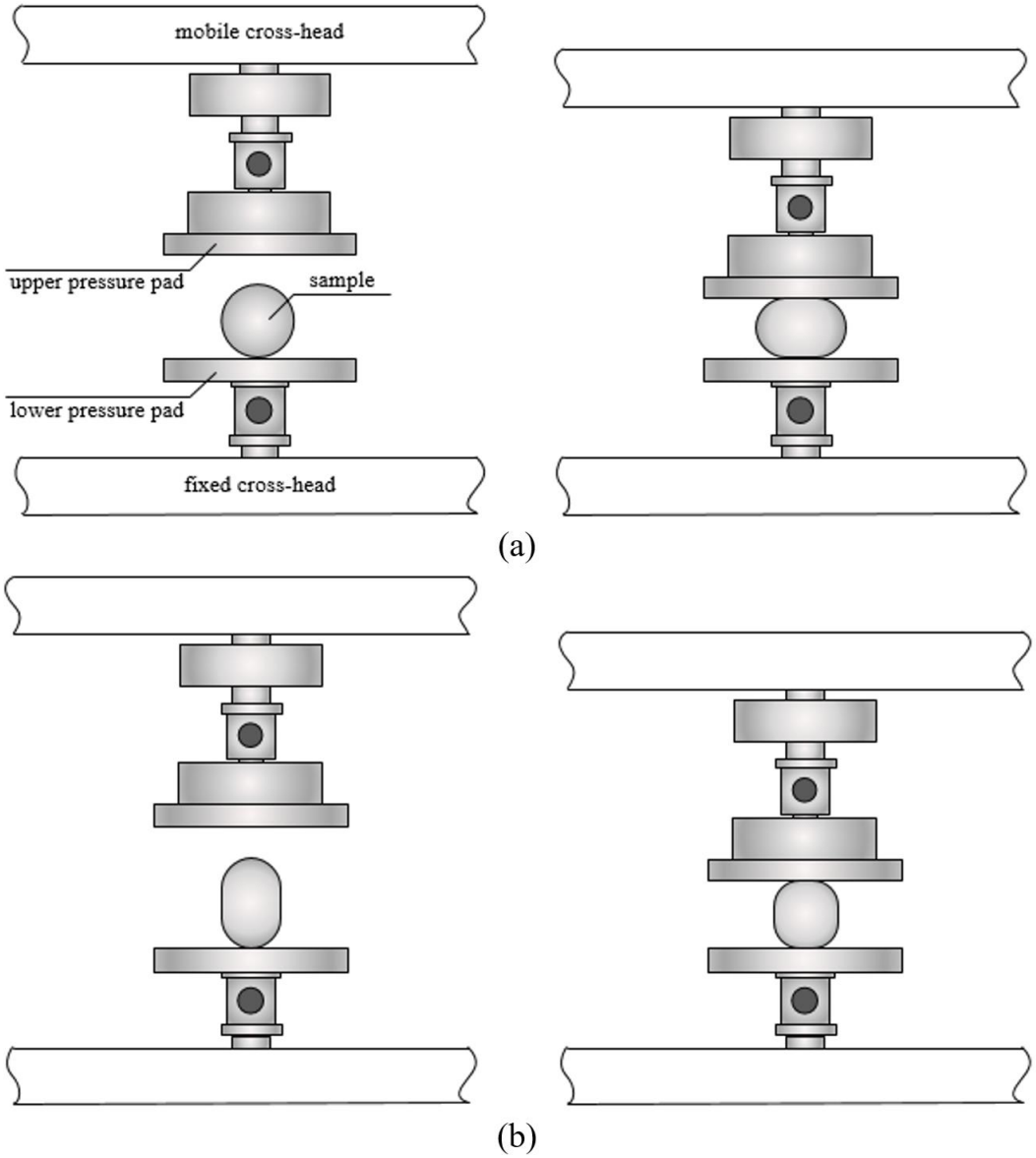

Fig. 6 a) The first and b) the second compression test

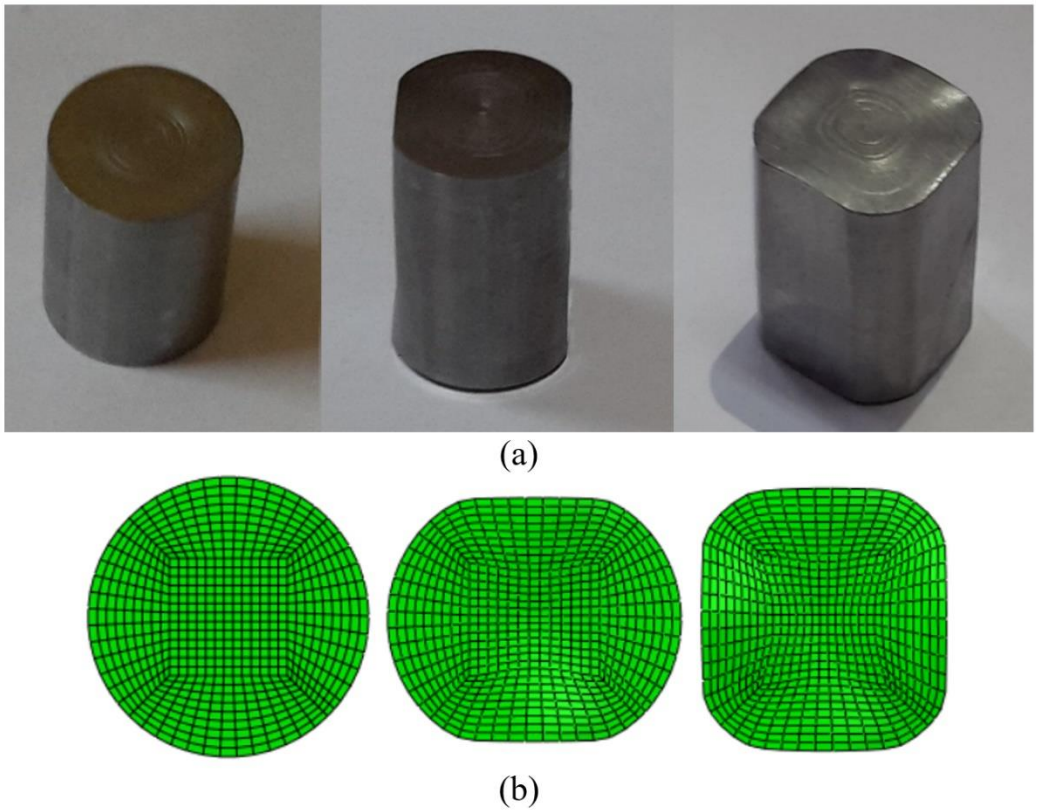

Fig. 7 a) The sample shaped in compression tests, b) the part shaped in the FEM model of the equivalent radial forging process

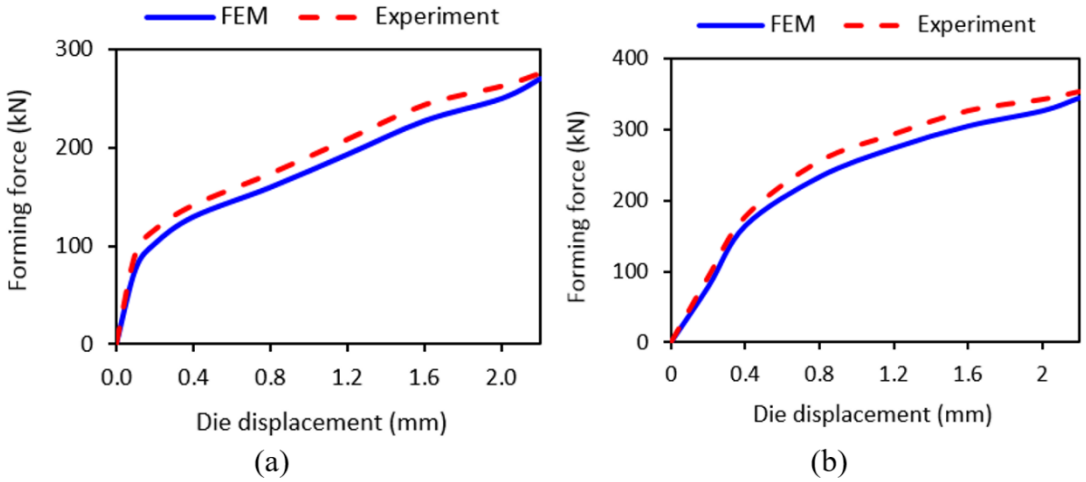

Fig. 8 The forming force in a) the first and b) second hit of dies

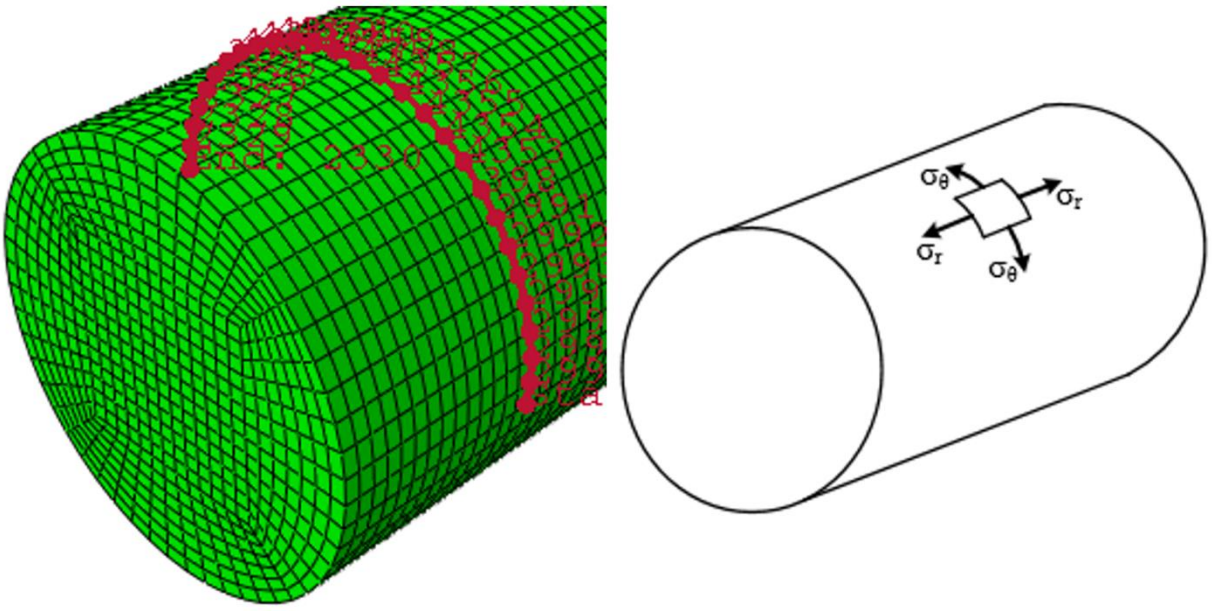

Fig. 9 a) A 3D plot of the path on which results are presented, b) definition of hoop stress (σ_θ) and axial stress (σ_r)

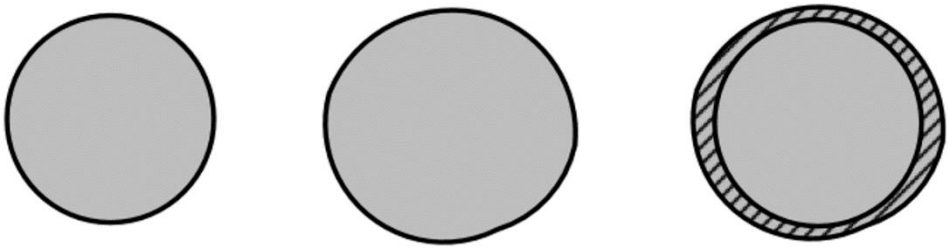

Fig. 10 Hypothetical cross section of a) the desired product, b) the forged part and c) overprinted cross sections and hatched area

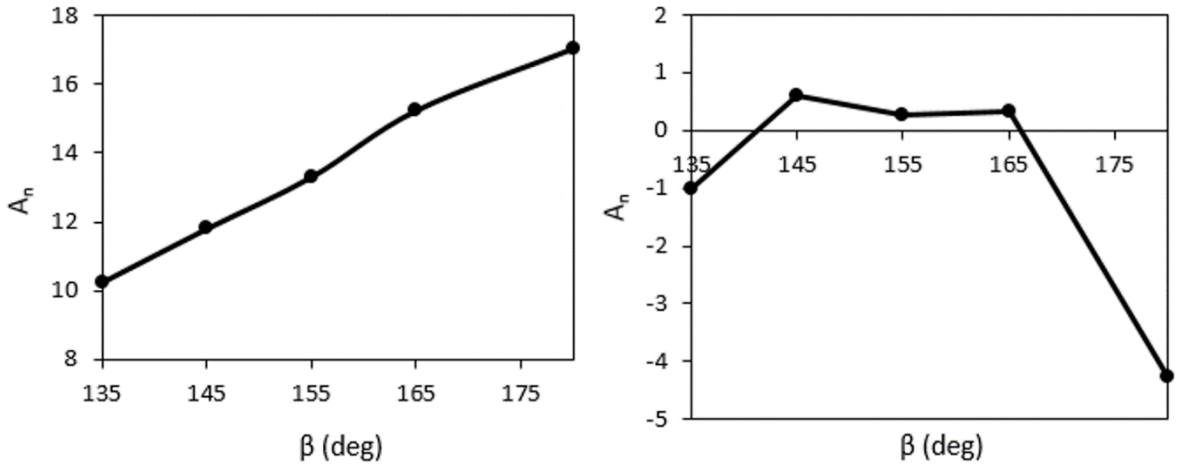

(a) (b)

Fig. 11 Variation of A_n with β a) after two hits of dies and b) after a complete circle rotation of the part

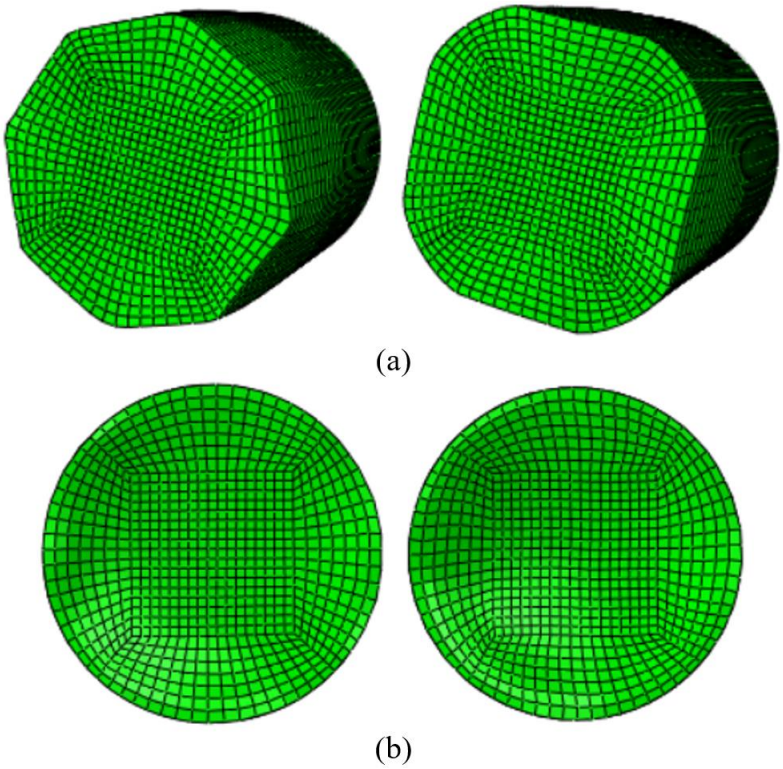

(a)

(b)

Fig. 12 a) Parts shaped by two hits of dies with $\beta = 135^{o}$ (left) and $\beta = 180^{o}$ (right) and b) Part cross section after a complete rotation for $\beta = 135^{o}$ (left) and $\beta = 180^{o}$ (right)

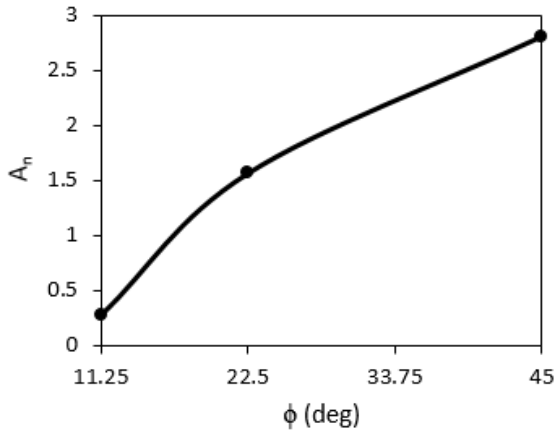

Fig. 13 Diagram of A_n variation with rotational feed angle

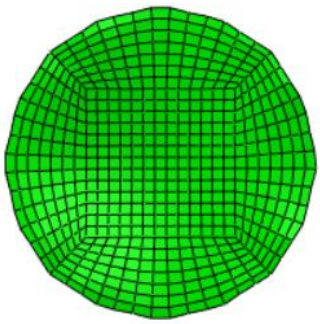

Fig. 14 Part cross section after a complete rotation for $\phi = 45^{o}$

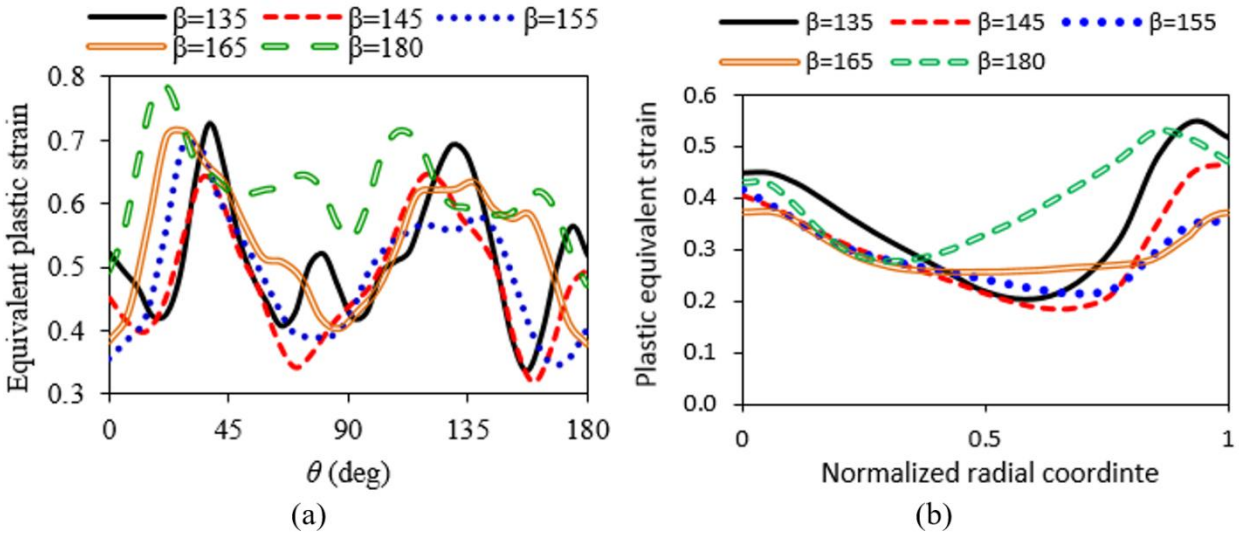

Fig. 15 Diagram of equivalent plastic distribution in a) the hoop direction in the surface and b) the radial direction

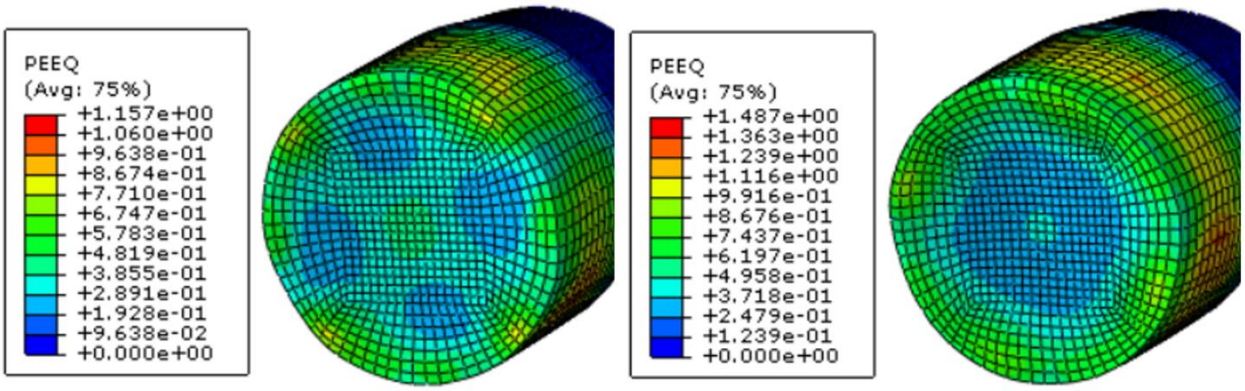

(a) (b)

Fig. 16 Contour of the equivalent plastic strain in the part forged by a die with a) $\beta = 135^{o}$ and b) $\beta = 180^{o}$

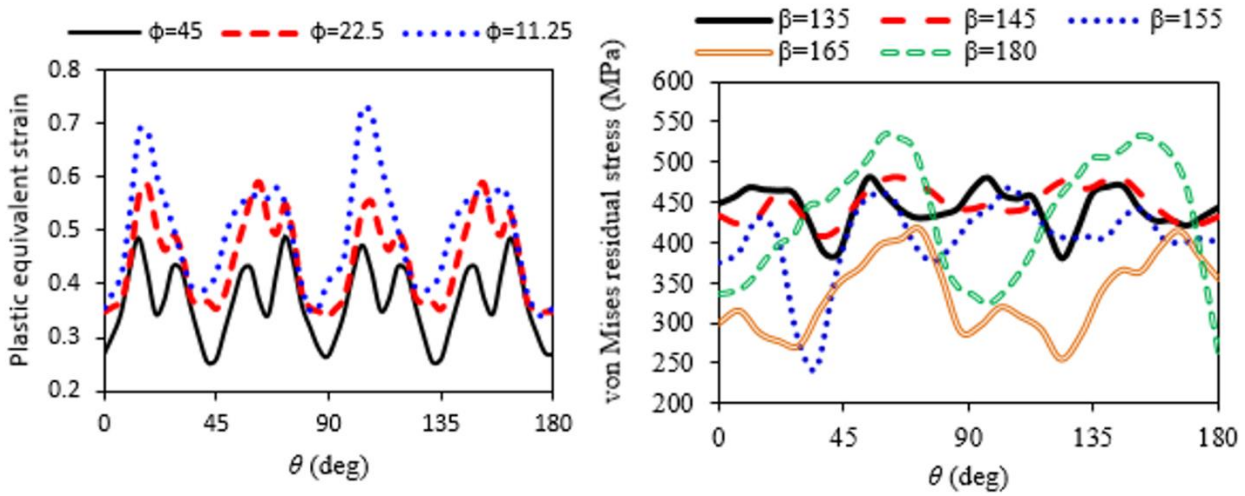

(a) (b)

Fig. 17 Diagram of a) the plastic strain and b) in the von Mises residual stress distribution in the part surface

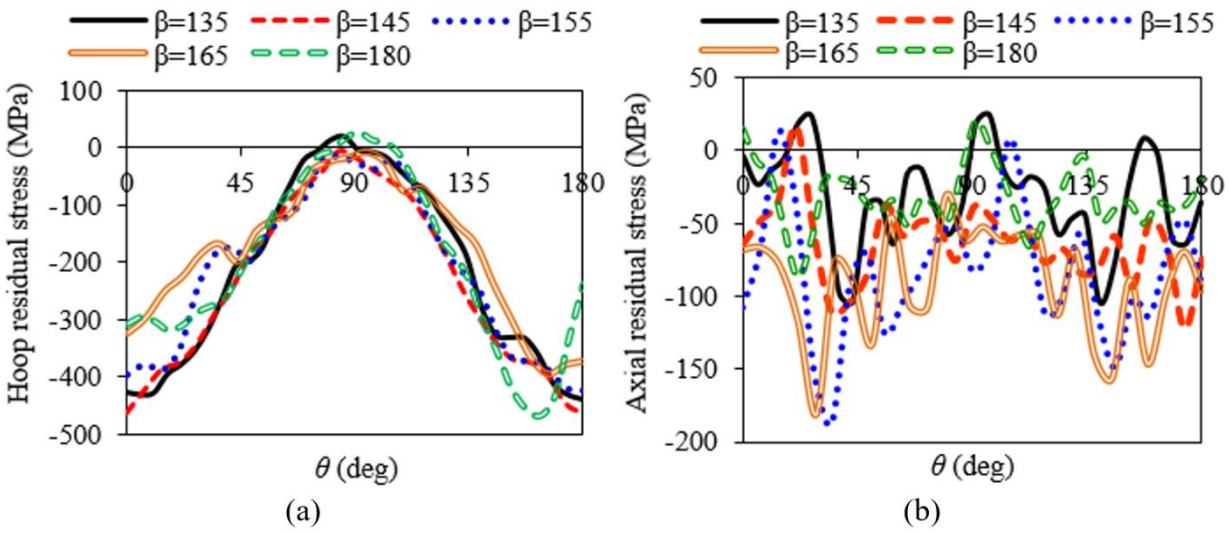

Fig. 18 Diagram of a) the hoop residual stress and b) the axial residual stress in the part surface

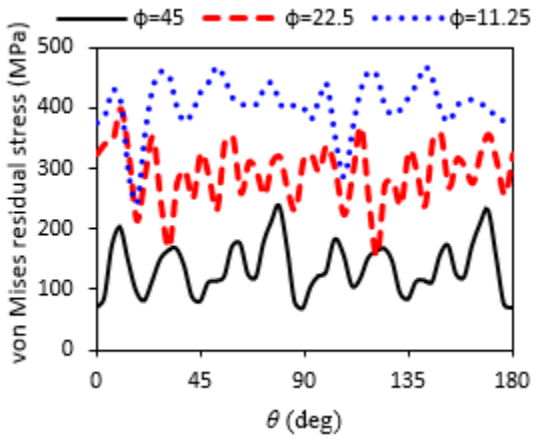

Fig. 19 Diagram of the von Mises residual stress in the part surface for different rotational feeds

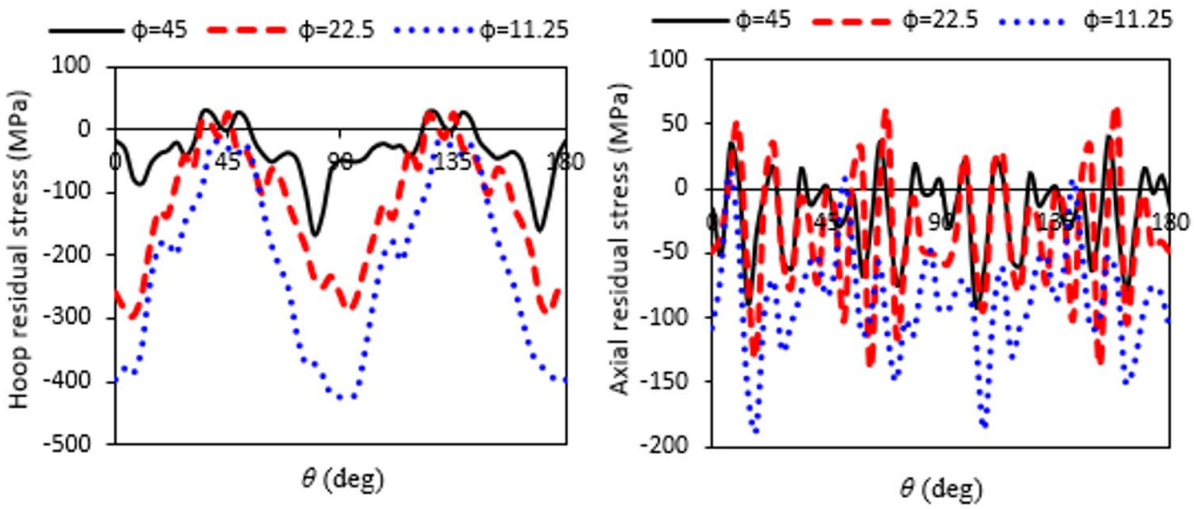

(a) (b)

Fig. 20 Diagram of a) the hoop residual stress and b) the axial residual stress in the part surface for different rotational feeds

Table 1 The values considered for the die transverse angle β and the part rotational feed angle ϕ

β (deg)	ϕ (deg/stroke)
135	11.25
145	22.5
155	45
165	0.19
180	0.37

Mozhdeh Fattahpoor Roushan received her B.S and .M.S. degrees both in mechanical engineering from Babol Noshirvani University of Technology, Iran, in 2014 and 2016, respectively. She is currently a Ph.D. student at the same university. Her main research interests are finite element simulation and modeling of metal forming processes.

Hamed Afrasiab received his B.S., M.S. and Ph.D. degrees all in mechanical engineering from Sharif University of Technology, Iran, in 2004, 2006 and 2011, respectively. He is currently an associate professor at the department of mechanical engineering, Babol University of Technology, Iran. His main research interests are mechanics of fuel cell components, finite element method, composite materials, sandwich structures, and modeling of metal forming processes.

Ramazan-Ali Jafari-Talookolaei is currently an assistant professor at the Department of Mechanical Engineering, Babol Noshirvani University of Technology, Iran. He received his B.Sc. in Mechanical Engineering from Shahrood University of Technology in 2002, and his M.Sc. and Ph.D. degrees in Mechanical Engineering from Sharif University of Technology, in 2004 and 2013, respectively. His main research interests are Laminated Composite Structures, Finite Element Method, Vibrations, and Damaged Structures.